

# Towards Smart Fronthauling Management: Experimental Insights from a 5G Testbed

Marcello Morini<sup>1</sup>, Eugenio Moro<sup>1</sup>, Ilario Filippini<sup>1</sup>, Danilo De Donno<sup>2</sup>, Salvatore Moscato<sup>2</sup>, Antonio Capone<sup>1</sup>

<sup>1</sup> DEIB, Politecnico di Milano, Milan, Italy - {name.surname}@polimi.it

<sup>2</sup> Milan Research Center, Huawei Technologies Italia S.r.l., Milan, Italy - name.surname@huawei.com

**Abstract**—The fronthaul connection is a key component of Centralized RAN (C-RAN) architectures, consistently required to handle high capacity demands. However, this critical feature is at risk when the transport link relies on wireless technology. Fortunately, solutions exist to enhance the reliability of wireless links. In this paper, we recall the theoretical fronthaul model, present a dynamic reconfiguration strategy and perform a conclusive experiment. Specifically, we showcase the setup of a wireless fronthaul testbed and discuss the resulting measurements. For this task, we leveraged the commercial hardware provided by the High-Frequency Campus Lab (HFCL), a private 5G network with millimeter wave (mmWave) radio access interface. Our experiments provide original data on the fronthaul utilization in this real deployment, demonstrating both a good accordance with the theoretical model discussed in [1] and the viability of one stabilizing solution.

## I. INTRODUCTION

The Centralized RAN paradigm is reshaping cellular networks with disruptive force. The emphasis on decentralization, particularly within the framework of Open RAN (O-RAN), underscores its anticipated fundamental role in the future of cellular networks. Operators and the industry at large are recognizing the value of decentralization, driving advancements that offer significant benefits in network flexibility and efficiency. Radio Access Network (RAN) decentralization techniques streamline site engineering and provide revolutionary deployment flexibility opportunities. Modern Ethernet-based fronthaul interfaces, such as Enhanced Common Public Radio Interface (eCPRI) and O-RAN Open Fronthaul, facilitate this flexibility, allowing operators to rethink their transport networks and introduce heterogeneity. This capability to reimagine transport networks is remarkably helpful in optimizing network performance and cost.

The newly introduced flexibility enables operators to explore transport network alternatives to dedicated fibers[2], including E-band radio links, extremely high-frequency point-to-multipoint radio links, and even free-space optics. These alternatives present a promising reduction in capital and operational expenditures, especially in areas where new fiber deployment is prohibitively expensive. The wireless-vs-wired technology comparison in [3] shows that, in appropriate conditions, wireless technologies can provide sufficient link capacity at a cost even lower than wired counterparts. However, despite these cost benefits, alternative wireless approaches often need to improve reliability compared to dedicated fiber connections. Due to adverse atmospheric conditions, high-frequency fronthaul links and Free Space Optics are susceptible to link quality degradation. Additionally, packet-switched fronthaul

networks are vulnerable to congestion, further complicating their deployment.

Traditionally, the reliability issue in wireless fronthaul links has been mitigated by over-dimensioning, a strategy that is inefficient and costly, negating many of the positive aspects of alternative solutions. Adaptive solutions present a more efficient and cost-effective approach. Previous work by the authors has introduced a dynamic and adaptive mechanism that manages instantaneous access resources to accommodate transitory fronthaul capacity reductions caused by effects such as rain [1]. The potential demonstrated by the simulations justifies a comprehensive set of practical experiments, which is the focus of this paper.

To perform measurement campaigns, authors leveraged High-Frequency Campus Lab (HFCL): a standard-compliant private 5G testbed, designed to support rigorous experiments. This network comprises a macro 5G Next Generation Node Base (gNB) operating at millimeter wave (mmWave), covering Politecnico di Milano campus and the surrounding neighborhood. The base station is dedicated solely to research and experimentation, ensuring high experimental repeatability. The high capacity of mmWave let us test the fronthaul connection under extreme access loads. The deployed hardware and tailored setup facilitate testing across a broad range of controlled conditions. This setup positions HFCL as one of the few facilities worldwide capable of precisely replicating typical adverse atmospheric effects on advanced mmWave 5G networks.

In this work, we revisit the theoretical foundations of fronthaul rate adaptation mechanisms and describe two experiments applying these principles in a real network environment. Specifically, the first experiment demonstrates the feasibility of the *Cell Reconfiguration* strategy, while the second validates the theoretical fronthaul rate model presented in [1]. This study aims to provide the first insights into the real-world performance of fronthaul systems in front of varying channel conditions that lead to capacity reduction, potentially contributing to more effective wireless Centralized RAN (C-RAN) deployments.

The paper is structured as follows. The next section provides context on C-RAN fronthaul and section II discussed the available literature on this theme. Section IV reviews theoretical fronthaul rate model and adaptation strategies. The experimental section follows, detailing the testbed setup in Section V and the experiments in Section VI. Finally, Section VII concludes the paper.

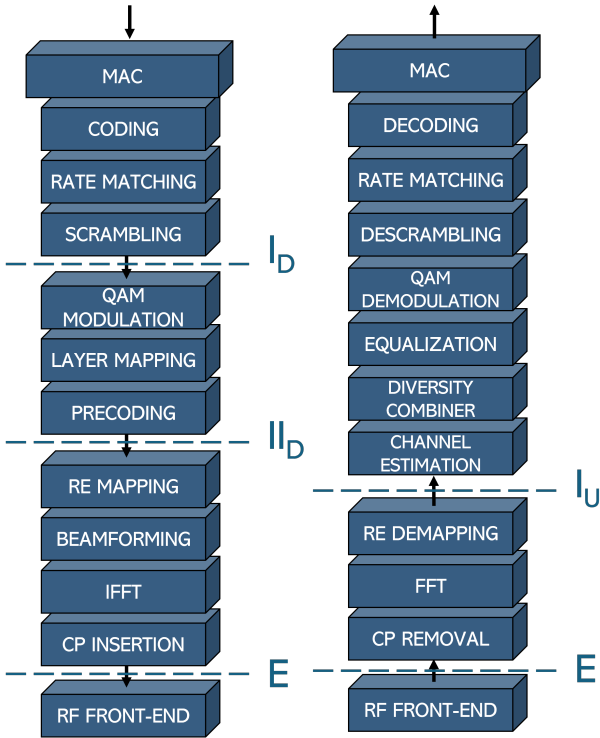


Fig. 1: Physical layer functions chain and eCPRI splits [4]

## II. BACKGROUND ON C-RAN AND FUNCTIONAL SPLITS

The 5G gNB implements an extensive chain of network functions. Part of this chain, namely the physical layer functions, are reported in Figure 1, for both Uplink (UL) and Downlink (DL) directions. Not all the functions are implemented in the same physical device, but they are split between two separate entities, connected via a fronthaul link. Depending on the reference architecture, these two entities have been named either Active Antenna Unit (AAU) and Base Band Unit (BBU), or Radio Unit (RU) and Distributed Unit (DU). The decision where to implement specific functions is known as *split option*. Among the possible splits, the eCPRI standard defines five options – three for DL and two for UL – shown in Figure 1. For instance, if the network configuration chooses split option  $I_D$ , all functions from the RF front-end to the QAM modulation are implemented in the AAU, while higher-layer functions are handled in the BBU. Recently, O-RAN Alliance has introduced additional split options, which expand upon the eCPRI-defined options [5].

Depending on the chosen split, different types of data are transmitted over the fronthaul. For example, basic bits are transmitted at split option  $I_D$ , while IQ symbols – specifically bit-encoded IQ symbols – are found at option  $II_D$ . Generally, the fronthaul data rate (or fronthaul rate) increases as the split moves from higher to lower layers in the chain, eventually saturating at *split E*. At this level, all unused Resource Block (RB) are zero-padded, and the rate, reaching its peak, becomes constant. This behavior contrasts with splits above E, where the fronthaul rate depends on the data requested by users. This principle underpins the model presented in [1] and partially

reviewed in Section IV. While latency and coordination requirements also vary across split options, this paper wants to analyze the feasibility of adaptation techniques for wireless fronthaul, therefore these aspects fall outside the scope of this paper. In this context, understanding how to model fronthaul link capacity – and the extent to which real implementations align with these models – is crucial.

## III. RELATED WORKS

This paper investigates the dynamic reconfiguration of 5G cells to adapt to variable fronthaul capacity in wireless links. In this section, we address both the broader context of our research – covering the theoretical foundations of C-RAN splits and RAN reconfiguration strategies – and the availability of testbeds for the practical evaluation of the fronthaul aspects, which is our primary focus.

Various studies have investigated the requirements of C-RAN splits. For instance, [6] offers a comprehensive review of different functional splits, ranging from low-PHY to PDCP/RRC, highlighting their pros and cons along with formulas for estimating fronthaul rate requirements. Additionally, [7] presents simulation data to illustrate typical fronthaul rate needs. Building on these foundational works, [1] introduces a more general and updated model, providing new insights into fronthaul rate dimensioning. While these references offer critical theoretical context, they do not explore practical implementations.

Research on RAN reconfiguration underscores the potential to adjust C-RAN splits and resources to meet various requirements, such as power, latency, and fronthaul capacity. The concept of *Joint Access and Fronthaul Coordination* has been examined as both a static optimization problem [8], and a time-varying one [9], [10], [11]. While we acknowledge and share some foundational ideas from this research, the introduction of flexible splits complicates the reconfiguration process significantly. In contrast, our approach focuses specifically on modifying MIMO layers and resource blocks, offering a simpler strategy that can be readily implemented in commercial systems.

Real-world testbeds remain underexplored. Notable contributions include [12] and [13], which focus on fiber-based fronthaul deployments. The work in [12] presents an OAI-based testbed to evaluate fronthaul rate, latency, and jitter, while [13] measures data rate and processing power for various splits. The most recent study, [14], combines modeling with experiments on a fixed-capacity wireless fronthaul link.

While these studies offer valuable insights, our work distinguishes itself by focusing on a fronthaul testbed constructed with commercial hardware. This emphasis on practical evaluation addresses a gap in the literature, enhancing the understanding of fronthaul performance in commercial 5G deployments through a comprehensive set of measurements.

In summary, while previous literature has established the theoretical and conceptual groundwork, this paper advances the state of the art by providing a comprehensive analysis of fronthaul performance on a testbed utilizing commercial

equipment. This work helps bridge the gap between theory and practical application in CRAN architecture.

#### IV. FOUNDATIONS OF RADIO ACCESS RECONFIGURATION

To provide theoretical foundations to the management strategies that are the focus of the experiments, this section discusses a fronthaul rate model. This model derives from [1] and only reports the formulas for *split*  $I_D$  and  $I_U$ .

The rates that the fronthaul link must support are:

$$R_{FH}^{I_D} = N_{RB} \cdot N_{SC} \cdot N_{MIMO} \cdot Q_M \cdot \frac{1}{T_S}, \quad (1)$$

$$R_{FH}^{I_U} = N_{RB} \cdot N_{SC} \cdot N_{MIMO} \cdot N_{IQ} \cdot \frac{1}{T_S}, \quad (2)$$

for the DL and the UL, respectively. Both formulas consider:  $N_{RB}$ , the number of used RBs by the radio access interface,  $N_{SC}$ , the number of subcarriers per RB (i.e., twelve),  $N_{MIMO}$ , the number of concurrently active Multiple Input, Multiple Output (MIMO) layers, and  $T_S$ , the duration of an OFDM symbol. Two parameters differ between the two formulas above:  $Q_M$ , which represents the number of bits per modulated by each symbol, and  $N_{IQ}$ , the number of bits used to encode an IQ sample (i.e., the bitwidth). In other words, this means that the DL fronthaul carries flows of raw data bits while the UL fronthaul carries bit-encoded IQ symbols. Since  $N_{IQ}$  is usually bigger than  $Q_M$ , the UL fronthaul rate is usually higher than the DL counterpart.

It is important to note that these formulas include an approximation. Beyond the Resource Element (RE) data, the fronthaul link must also carry antenna control information, with beamforming control being particularly significant. Further details on this aspect are available in [1]. We do not consider this contribution further in the paper, as it is highly implementation-dependent. However, its impact is expected to be minor in our testbed, which uses hybrid beamforming and thereby significantly reduces the antenna control information compared to full-digital beamforming.

The fronthaul link capacity must always meet or exceed the rates calculated for  $N_{RB} = N_{RB}^{MAX}$  and  $N_{MIMO} = N_{MIMO}^{MAX}$ , representing the maximum number of active RBs and MIMO layers in the radio access configuration. Ensuring this constraint is typically manageable when dedicated optical fiber links are used for transport; however, it becomes a significant technical challenge when links are wireless or fiber is shared, as link capacity is no longer under the designer's control.

If the fronthaul capacity falls short of the rate requirements, the system may attempt to maintain an effective fronthaul connection by adjusting access resources, leveraging the relationship between access and fronthaul. Specific countermeasures can limit the number of RBs,  $N_{RB}$ , and MIMO layers,  $N_{MIMO}$ , available to the gNB's scheduler [1]. In particular, the *cell reconfiguration* can be implemented by selectively disabling certain radio access resources through software reconfiguration. This impacts the total radio access capacity according to the formula [15]:

$$R_{ACC} = N_{RB} \cdot N_{SC} \cdot N_{MIMO} \cdot Q_M \cdot R_{MAX} \cdot f_{TDD} \cdot \frac{(1 - OH)}{T_S}$$

<b>AAU coordinates (lat,lon,h)</b>	45.478671, 9.232550, 22 m
<b>Central AAU azimuth, down tilt</b>	135°, 2°
<b>Center frequency</b>	27.2 GHz (n257)
<b>Max channel bandwidth</b>	200 MHz
<b>Subcarrier spacing</b>	120 kHz
<b>TDD Frame structure</b>	4:1 (DDDSU)
<b>Maximum modulation (DL/UL)</b>	256 QAM/64 QAM
<b>Transmit power</b>	37.5 dBm
<b>Gain</b>	32.5 dBi
<b>Effective Isotropic Radiated Power</b>	70 dBm
<b>Maximum MIMO layers</b>	8T-8R
<b>Split (DL/UL)</b>	$I_D/I_U$

TABLE I: Active Antenna Unit configuration parameters

<b>CPE model</b>	Huawei H312m-371
<b>Chipset</b>	Huawei Hisilicon Balong 5000
<b>Max EIRP [dBm]</b>	40
<b>MIMO layers</b>	2T-2R
<b>Antenna</b>	Planar array
<b>QAM order (DL/UL)</b>	64/64

TABLE II: Customer Premises Equipment characteristics

where  $R_{MAX}$  is the target code rate,  $OH$ , is the overhead due to the control channels (e.g., PBCH, PRACH), and  $f_{TDD}$ , is a factor dependent on the Time Division Duplexing (TDD) frame scheme (e.g., DDDSU) activated in the network.

An open issue remains in evaluating the impact and effectiveness of this strategy in a real network. In the next section, we present the experimental setup, and in Section VI, we demonstrate both the viability of *cell reconfiguration* and the consistency of the system behavior with Eq. 1.

#### V. EXPERIMENTAL SETUP

All the experiments were carried out at HFCL, an open, experimental network deployed in the campus of Politecnico di Milano. It consists of a standalone, private 5G network equipped with tools for measuring and testing its performance. Its deployment is the result of the joint effort of Politecnico di Milano, telecommunication companies, equipment manufacturers, and service companies, to enhance cooperation among researchers. The HFCL radio access interface operates only at mmWave and is only accessible from authorized Customer Premises Equipment (CPE). This allows us to produce high-fidelity 5G campaigns, excluding unwanted switching to other frequencies and interferences from external users.

##### A. System architecture and hardware

The full system used in the experiment is illustrated in Figure 2. The HFCL includes an Active Antenna Unit (AAU) *Huawei HAAU5323*, connected to a centralized Base Band Unit (BBU) *Huawei BBU5900*. The BBU is in turn wired to a 5G virtualized core network (not reported in the picture). This equipment is commercially available and the underlying technology is proprietary. However, the possibility to access the gNB configuration lets us modify many of its parameters, such as the access bandwidth, the Time Division Duplexing (TDD) structure and the transmitted power. Details on its configuration are reported in *Table I*.

The network is completed by a CPE working as User Equipment (UE), namely the *Huawei H312m-371*. Its main

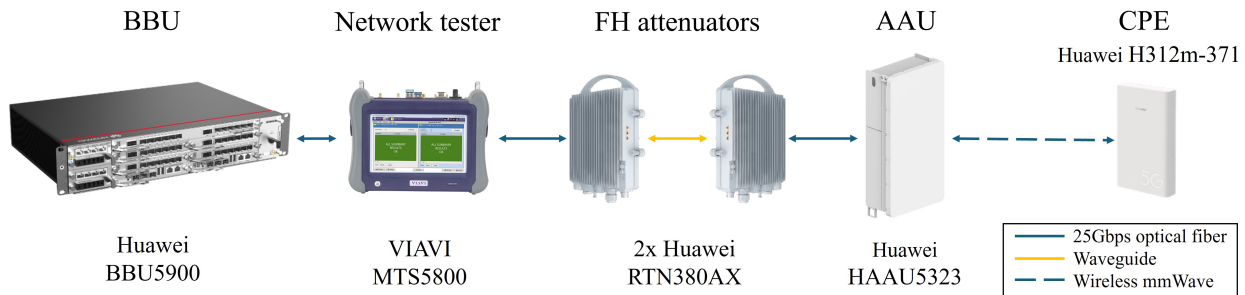


Fig. 2: High-Frequency Campus Lab RAN equipment involved in the experiment

Configurations	Channel bandwidth [MHz]	MIMO layers
1	200	4T-4R
2	100	4T-4R
3	100	8T-8R

TABLE III: Set of cell configurations

characteristics are reported in *Table II*. To collect data transfer logs (e.g., received signal power), we connect the CPEs to a PC running a *drive test log tool*, namely the CPE-compatible *Genex Probe 8.1* software.

To carry out fronthaul experiments, the 5G network was complemented by additional devices. In order to emulate wireless links' capacity variations in our optical fiber fronthaul, we placed two *Huawei RTN380AX* in the middle of the fronthaul optical connection. These are variable-rate transceivers working in the E-band (71–76 or 81–86 GHz) and usually employed in backhaul point-to-point connections. Among their features, they are capable to provide large capacities for wireless and support a wide set of channel bandwidths and modulations, that allow us adjusting E-band link capacity, symmetrically in both UL and DL, with a good granularity. In order to better confine and control the experiment, we connected the two transceivers with a waveguide instead of a free-space link. This optimizes space and allows high reproducibility of the experiments.

Finally, we included in the fronthaul chain a *VIAVI MTS-5800* network tester. This device was inserted between the BBU and the waveguide to measure the bitrate crossing the fronthaul link. We leveraged this reconfiguration capabilities in the experiments of Section VI.

## VI. EXPERIMENTAL RESULTS

The experimental campaign consists of two experiments: the implementation of an example of *cell reconfiguration* and a detailed *analysis of the fronthaul rate requirements*.

### A. Implementation of cell reconfiguration

This experiment aims to demonstrate the feasibility of *cell reconfiguration* adaptation strategy. To execute it, we leveraged two cell configurations: *configuration 1* and *2* reported in *Table III*.

The methodology used was the following. We enforced a bottleneck on the fronthaul capacity by setting different configurations of the E-band transceivers. By gradually increasing

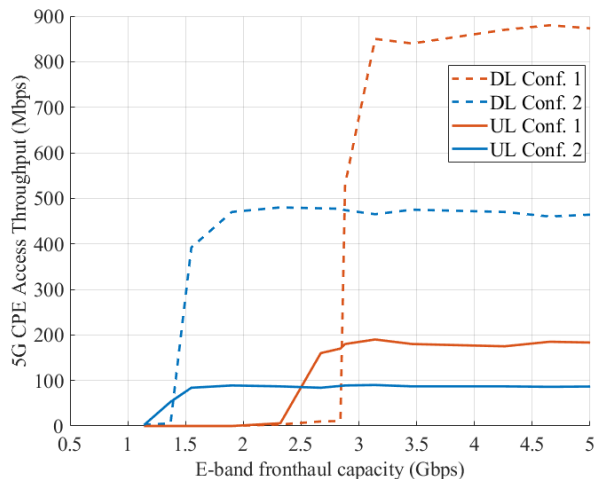
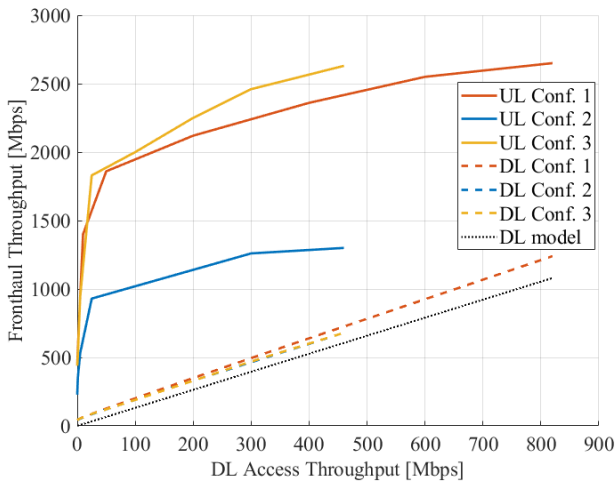


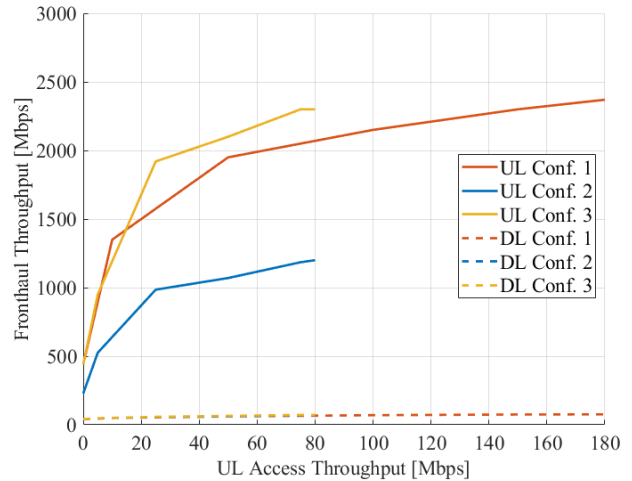
Fig. 3: Impact of Cell Reconfiguration on fronthaul rates

this capacity, we identified the minimum amount required to support the different cell configurations. We repeated this operation for each transmission direction and for every cell configuration. The results are shown in Figure 3, where the achievable access throughput is plotted against the available fronthaul capacity.

Configuration 1 shows that the UE can reach a DL rate of 850 Mbps if the fronthaul supports at least 3.1 Gbps. Similarly, the uplink saturates at around 200 Mbps when the fronthaul is greater or equal than 2.7 Gbps. The trends exhibit an on/off behavior: once a capacity threshold is reached, all available RBs are allocated to the UE, allowing it to achieve maximum throughput. In configuration 2, this pattern remains but is rescaled. The capacity threshold decreases to approximately 1.6 Gbps in both directions (i.e., about half of the previous case) at the cost of a halved access rate, which reaches 480 Mbps and 90 Mbps in DL and UL respectively. Configuration 2 allocates only half of the RBs,  $N_{RB}$ , available in configuration 1. This causes a reduction very close to a factor two not only in the achievable access rate but also in DL and UL required fronthaul capacities, as predicted by the Eqs. 1 and 2. The slight deviation from the exact halved value results from additional rates generated for antenna control, which are implementation-dependent. Overall, the system behavior aligns with expectations, demonstrating the viability of the



(a)



(b)

Fig. 4: Relation between fronthaul rate and access rate

cell reconfiguration strategy.

To further interpret the values in the plot, we conducted the following experiment.

#### B. Analysis on the fronthaul rate requirements

This experiment aims to deepen our understanding of fronthaul operations. Specifically, we show that for commonly considered fronthaul splits, the required fronthaul rate is closely linked to uplink traffic, with downlink traffic never acting as a bottleneck. For this analysis, we utilized all cell configurations listed in Table III.

We employed a methodology significantly different from the previous experiment. Without imposing any limitations on fronthaul capacity – allowing the E-band link to operate at full capacity – we used *iperf3* to generate arbitrary bitrate values between two PCs: one connected to the CPE and the other to the N6 interface of the Core Network (CN). This setup allowed us to observe how the generated bitrate translates over the fronthaul.

These values are shown on the x- and y-axes in Figure 4. Note that in each plot, the traffic is actively generated only in one direction (i.e., DL in Fig. 4a and in UL in Fig. 4b) yet fronthaul traffic also appears in the opposite direction. This is due to acknowledgments and control signals, which play a fundamental role.

In Figure 4a, the lines at the bottom of the graph indicate a linear relationship between the DL access throughput and the DL fronthaul throughput. The rates for configurations 2 and 3 increase linearly from the origin, reaching a point where access rate is 460 Mbps and fronthaul rate is 680 Mbps, at which point the UE utilizes all the RBs it can support. Although configuration 3 supports up to 8 MIMO layers, the UE is hardware-limited to 2 layers, so all 132 RBs are allocated to the CPE, with 66 per active MIMO layer [16]. Therefore, in the DL, configurations 2 and 3 perform similarly, each operating with a 100 MHz channel bandwidth.

Configuration 1, with a 200 MHz bandwidth, provides up to 132 RBs per MIMO layer, doubling the DL rates: DL access rate reaches 820 Mbps, and DL fronthaul rate reaches 1240 Mbps. These values closely align with those predicted by Equation 1, shown as the black line in the figure. The minor offset observed is attributed to antenna control data.

The UL curves in Figure 4a exhibit a markedly different behavior from those in the DL. First, fronthaul rate values are significantly higher in the UL than in the DL, even though UL access traffic mainly consists of acknowledgment traffic. This discrepancy arises from a lower UL functional split compared to the DL. Consequently,  $N_{IQ}$ -bit encoded symbols are transmitted over the UL fronthaul link rather than basic data bits, as is the case for the DL. It is difficult to estimate the exact value of  $N_{IQ}$  as it depends on dynamic compression algorithms.

Second, the UL exhibits two distinct regions: a steep rise at low access rates, driven by antenna control data, and a gradual increase at higher rates, where the impact of access resources becomes evident. This latter behavior reflects the bits carried in transmitted OFDM symbols across the whole bandwidth during a symbol period. Importantly, only symbols with no data across all subcarriers can be omitted from transmission over the fronthaul. Partially loaded OFDM symbols must be fully transmitted on the UL fronthaul link. This explains why, at low access rates, loaded symbols are primarily driven by signaling data, whereas at higher rates, the dependence on user data becomes more pronounced. Additionally, the slope of the curve is lower than in the DL case, as new resources – namely, additional symbols to be transferred through the fronthaul – are only needed once the currently used symbols are fully utilized.

Analyzing the three UL curves in Figure 4a, we observe that the values of configurations 2 and 3, which were equal in the DL, now differ by a factor of two at the same access rates. At their maximum access DL rate, configuration 2

achieves 1300 Mbps in the fronthaul, while configuration 3 reaches 2630 Mbps. This behavior is attributed to the number of available MIMO layers: used symbols are replicated across every antenna port and transmitted, irrespective of their activation in a specific layer. When comparing configuration 1 and configuration 3, instead, we find their fronthaul rates to be quite similar. Configuration 1 has double the bandwidth but half the MIMO layers compared to configuration 3. This aligns with Eq. 2: doubling  $N_{RB}$  and halving  $N_{MIMO}$  results in no change to the required fronthaul rate.

Overall, this indicates that transmitting RBs in UL necessitates sending a number of resources over the fronthaul link that is proportional to the product of total bandwidth and activated MIMO layers, accounting for all of RBs present in the same symbol period. However, calculating the exact number of RBs transmitted through the fronthaul is complex, as it depends on the scheduler's allocation of bits to symbols, influencing the resulting fully unloaded symbols that can be omitted.

In Figure 4b, an arbitrary UL throughput is enforced in the access via *iperf3*. The trends observed previously are extended here, with a significant contribution from the UL traffic and a minor contribution from the resulting DL traffic. The latter occupies a negligible share of the bandwidth, while the former remains the dominant contribution. Notably, the maximum UL fronthaul occupancy remains similar to that in Figure 4a, despite the UL access traffic being pushed to 180 Mbps in this scenario, compared to the acknowledgment traffic generated by an 850 Mbps DL connection in the previous figure.

One final observation clarifies the results obtained in the *cell reconfiguration* experiment. Referring back to the thresholds in Figure 3, we can now conclude that these thresholds are dictated by the UL transmission, which requires approximately 2650 Mbps for an 850 Mbps DL access rate, rather than by the DL transmission, which only necessitates 1240 Mbps.

The experiment reported in this section demonstrates, through real measurements, the feasibility of the *cell reconfiguration* strategy and the overall correctness of Eqs. 1 and 2 in describing the fronthaul resource requirements. While downlink fronthaul rates are easily predictable, UL fronthaul rates are significantly influenced by the implementation of the eCPRI fronthaul interface and the scheduling policy governing access traffic. Overall, our system demonstrates that fronthaul management for downlink traffic using *split I<sub>D</sub>* is highly efficient, while the *split I<sub>U</sub>* for uplink traffic is more resource-intensive, representing the primary limitation during a reduction in fronthaul capacity.

## VII. CONCLUSIONS

In this paper, we explored the dynamic reconfiguration of 5G cells to adapt to variable fronthaul capacities in wireless links, focusing on the theoretical underpinnings of C-RAN splits and RAN reconfiguration strategies. Through comprehensive measurements conducted on a testbed built with commercial hardware, we provided valuable insights into fronthaul performance and its implications for real-world 5G deployments.

Our findings demonstrate that the fronthaul management for downlink traffic implementing *split I<sub>D</sub>* is highly efficient, while the uplink *split I<sub>U</sub>* proves to be more resource-intensive and serves as a critical limitation under reduced fronthaul capacity conditions. The experimental results validate the accuracy of our proposed models, particularly Eqs. 1 and 2, in characterizing fronthaul resource requirements.

Moreover, we established that the required fronthaul rates are predominantly influenced by uplink traffic, highlighting the need for careful consideration of scheduling policies and the implementation of eCPRI interfaces. This work not only advances the theoretical understanding of fronthaul dynamics but also bridges the gap between theory and practical applications, providing a foundation for future research in adaptive strategies for 5G networks.

## ACKNOWLEDGMENTS

The research in this paper has been carried out in the framework of Huawei-Politecnico di Milano Joint Research Lab.

## REFERENCES

- [1] M. Morini, E. Moro, I. Filippini, D. D. Donno, and A. Capone, "Shaping radio access to match variable wireless fronthaul quality in next-generation networks." <https://arxiv.org/abs/2406.15899>, 2024.
- [2] M. Jiang, J. Cezanne, A. Sampath, O. Shental, Q. Wu, O. Koymen, A. Bedewy, and J. Li, "Wireless fronthaul for 5g and future radio access networks: Challenges and enabling technologies," *IEEE Wireless Communications*, vol. 29, no. 2, pp. 108–114, 2022.
- [3] I. Sousa, N. Sousa, M. P. Queluz, and A. Rodrigues, "Fronthaul design for wireless networks," *Applied Surveys*, vol. 10, no. 14, 2020.
- [4] Ericsson AB, Huawei Technologies Co. Ltd, NEC Corporation and Nokia, "eCPRI Specification V2.0," tech. rep., 2019-05-10.
- [5] O-RAN Alliance, Working Group 4 (Open Fronthaul Interfaces WG), "Control, Split and Synchronization Plane Specification, 0-R003-v13.00," tech. rep., 2023.
- [6] L. M. P. Larsen, A. Checko, and H. L. Christiansen, "A survey of the functional splits proposed for 5g mobile crosshaul networks," *IEEE Communications Surveys & Tutorials*, vol. 21, no. 1, pp. 146–172, 2019.
- [7] Small Cell Forum, "Darts - an analysis tool for disaggregated ran transport," tech. rep., 2023.
- [8] S. Matoussi, I. Fajjari, S. Costanzo, N. Aitsaadi, and R. Langar, "5g ran: Functional split orchestration optimization," *IEEE Journal on Selected Areas in Communications*, vol. 38, no. 7, pp. 1448–1463, 2020.
- [9] A. Martínez Alba and W. Kellerer, "Dynamic functional split adaptation in next-generation radio access networks," *IEEE Transactions on Network and Service Management*, vol. 19, no. 3, pp. 3239–3263, 2022.
- [10] C.-F. Liu, S. Samarakoon, and M. Bennis, "Fronthaul-aware software-defined joint resource allocation and user scheduling for 5g networks," in *2016 IEEE Globecom Workshops (GC Wkshps)*, pp. 1–6, 2016.
- [11] L. Li, M. Bi, H. Xin, Y. Zhang, Y. Fu, X. Miao, A. M. Mikaeil, and W. Hu, "Enabling flexible link capacity for ecpri-based fronthaul with load-adaptive quantization resolution," *IEEE Access*, vol. 7, pp. 102174–102185, 2019.
- [12] G. Mountaser, M. L. Rosas, T. Mahmoodi, and M. Dohler, "On the feasibility of mac and phy split in cloud ran," in *2017 IEEE Wireless Communications and Networking Conference (WCNC)*, pp. 1–6, 2017.
- [13] A. I. Salama and M. M. Elmesalawy, "Experimental oai-based testbed for evaluating the impact of different functional splits on c-ran performance," in *2019 Novel Intelligent and Leading Emerging Sciences Conference (NILES)*, vol. 1, pp. 170–173, 2019.
- [14] D. Townend, R. Husbands, *et al.*, "Challenges and opportunities in wireless fronthaul," *IEEE Access*, vol. 11, pp. 106607–106619, 2023.
- [15] 3GPP, "NR; User Equipment (UE) radio access capabilities," Technical Specification (TS) 38.306, 3GPP, 03 2023. Version 17.4.0.
- [16] 3GPP, "NR; Base Station (BS) radio transmission and reception (Section 5.3.2)," Technical Specification (TS) 38.104, 3GPP, 02 2024. Version 17.12.0.